

# Time Domain Analysis of UWB Printed Monopole-Based Two-Port Systems for Characterization of On- to Off-Body Channels

*Elizabeth George, Debarati Ganguly, Debdeep Sarkar, Chinmoy Saha, Jawad Siddiqui, and Yahia Antar*

*Abstract* – This article entails a comprehensive approach to characterize an on-body to off-body ultrawideband (UWB) channel in time domain, considering a two-port UWB monopole antenna system working over the 2 GHz to 12 GHz frequency band. The various time domain figures of merit, such as the radiated–received pulses, power spectral densities (PSDs) of the transmit–receive pulses, ringing, fidelity, and group delay for the on-body transmit and off-body receive system lay the foundation for UWB channel modeling based on a pulse dispersion estimation. The proposed approach is systematically validated by extensive full-wave simulation results by using CST Microwave Studio, version 2018, along with real-time experiments with human volunteers. The pulse dispersion estimation–based channel modeling strategy can work as a handy alternative to traditional techniques with fading statistics or empirical tap delay models.

## 1. Introduction

In the present wireless age, body area network systems are of paramount importance due to the application in various fields, including sports, health care, multimedia [1], and indoor data transmission systems [2]. Although a plethora of wireless communication bands, such as BCS (5 Hz to 50 Hz), MICS (402 Hz to 405 Hz), WMTS (420 Hz to 450 Hz and 863 Hz to 870 Hz), and the mainly used ISM bands (902 Hz to 928 Hz and 950 Hz to 956 Hz) exist for authorized deployment of body-centric wireless communication services (BCWCs), the authorized minimally invasive ultrawide bandwidth (UWB) from 3 GHz to 10 GHz provides some attractive features, including low power spectral density (PSD), low interference, being less prone to fading, and high data rates [3]. Moreover, the low power transmission requirements find wide applications for wireless nodes worn on or in close proximity

to the body [3]. The inherent challenge lies in the choice and design of the on-body UWB antenna, as on-body channel modeling involves indelible challenges such as antenna–body interactions due to body movements and body shadowing effects for nonline-of-sight (NLOS) channels leading to degradation of radiation efficiency and radiation pattern of the on-body antenna. Thus, the antenna gain decreases, but its directivity increases, resulting from reflections of the body [3].

Over the years, many aspects of the UWB BCWC have been thoroughly documented in both stochastic and experimental realms [4–14]. The parameter that has been estimated by various research groups for UWB channel modeling is the channel impulse response (CIR), a direct figure of merit for time domain analysis that is the indelible feature of any ultrawideband system [8, 13].

In this article, a two-fold approach has been presented for analyzing on-body to off-body channel modeling: 1) an indoor scenario line-of-sight (LOS) on-body to off-body experimental setup involving two identical UWB monopole antennas operating in the recommended bandwidth of the Federal Communications Commission, 3 GHz to 10 GHz; 2) an extensive simulation setup to characterize the channel between an on-body and off-body UWB antenna in terms of time domain characteristics of the transmit–receive antenna by using [15, 16]. The novelty of the proposed approach is that an on-body UWB channel can be characterized in terms of pulse dispersion. The proposed approach, after being tested for NLOS, reverberant, and multipath environments can serve as an alternate and simplified methodology for estimation of UWB on-body–off body channels without involving stochastic modeling or path loss model.

## 2. Antenna and Phantom Model Design

Two similar antennas have been used for on-body to off-body measurements. The planar UWB circular monopole ( $L \times W = 50 \text{ mm} \times 50 \text{ mm}$ ) with a diameter of 25 mm, printed on a dielectric laminate having  $\epsilon_r = 2.33$  and  $\tan \delta = 0.00012$ , acts as both transmitting (Tx) and receiving (Rx) antennas. The off-body antenna, Ant-2, serves as the Rx antenna, whereas the phantom model, the Tx antenna, is named Ant-1. The position of the Rx is varied to orient it suitably in the near and far field of the Tx for respective cases. The onset of the far field is obtained by the rule of thumb  $2D^2/\lambda$ , with  $D$  being the largest dimension of the antenna under consideration and  $\lambda$  being the wavelength correspond-

Manuscript received 1 September 2020.

Elizabeth George and Chinmoy Saha are with the Department of Avionics, Indian Institute of Space Science and Technology, Trivandrum, Kerala - 695547, India; e-mail: elisakattackal@gmail.com.

Debdeep Sarkar is with the Department of Electrical and Communication Engineering, Indian Institute of Science, Bengaluru, Karnataka - 560012, India; email: debdeep@iisc.ac.in.

Debarati Ganguly, Jawad Siddiqui, and Yahia Antar are with the Department of Electrical and Computer Engineering, Royal Military College, Kingston, ON - K7K 7B4, Canada; e-mail: dgs.rpe@gmail.com.

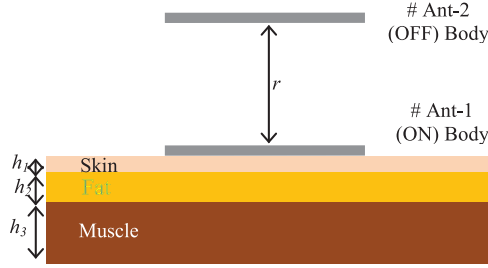


Figure 1. Schematic of the arrangement of an on-body UWB monopole Tx mounted on a three-layered human phantom arm and an off-body UWB monopole antenna in receiving mode placed at far field at a distance  $r$ . The heights of each layer are  $h_1 = 5$  mm,  $h_2 = 10$  mm, and  $h_3 = 30$  mm. The length of the tissue block is  $L = 100$  mm.

ing to the lowest frequency of operation. The three-layered human phantom arm model is designed with the respective effective permittivity and conductivity of each layer centered around 5.5 GHz. The top epidermal skin layer has a permittivity  $\epsilon_r = 35$  and  $\sigma = 3.46$  S/m, the middle fat layer has a permittivity  $\epsilon_r = 4.9$  and  $\sigma = 0.27$  S/m, and the bottom muscle layer has a permittivity of  $\epsilon_r = 49.4$  and  $\sigma = 4.8$  S/m [13, 17]. The Tx UWB monopole has been placed on the top epidermal layer as an on-body wearable antenna. The schematic of the previously mentioned arrangement is shown in Figure 1.

### 3. Results and Discussion

#### 3.1 Simulation Results and Time Domain Analysis

Initially, the stand-alone monopole, as shown in Figure 2, has been studied in a time domain to understand how the same antenna behaves when placed on the human phantom. The schematic for the arrangement of the on-body-off-body system for three different elevation angles,  $\theta = 0^\circ$ ,  $\theta = 60^\circ$ , and  $\theta = 90^\circ$ , are shown in Figures 3a–3c. For each case, the input signal for the on-body Tx antenna is chosen as a narrow monocycle pulse of pulse width of 400 ps, as it is devoid of any inherent ringing [18]. Figures 4a–4f show the frequency and time domain parameters, such as the radiated electric field sensed by a far-field probe and its associated ringing time interval  $\tau_r$ , PSDs of the input pulse, radiated pulse and received pulse, fidelity using a normalized cross correlation between the input and the received signals, and group delay characteristics. The same parameters are calculated for other elevation angles, as depicted in Figures 5 and 6. The radiated field of an UWB monopole is the inverted second temporal derivative of the input monocycle, shown in Figure 2b, for the stand-alone monopole, but the nature of the radiated field changes for the three case studies for on-body phantom models in Figures 4b, 5b, and 6b. This observation may be attributed to the lossy nature of the underlying three-layered phantom tending to change the effective permittivity of the substrate of the coplanar fed UWB monopole.

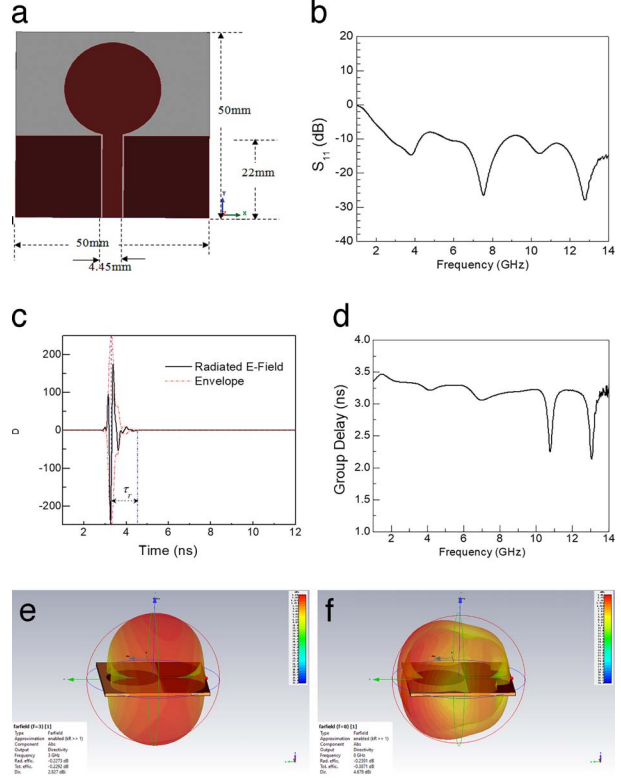


Figure 2. (a) Schematic of the stand-alone monopole to be used as an on-body transmit antenna and an off-body receive antenna. (b) Return loss characteristics of the stand-alone monopole. (c) Numerical computation of ringing; ringing interval  $\tau_r = 1.5$  ns. (d) Numerical computation of group delay by using MATLAB, version X [16]. (e) The 3-D radiation pattern at 5 GHz. (f) The 3-D radiation pattern at 8 GHz.

The group delay of the system and the pulse dispersion estimated by ringing interval  $\tau_r$  for three different cases of the on-body-off-body system do differ from that of the stand-alone monopole case. The  $\tau_r$  is

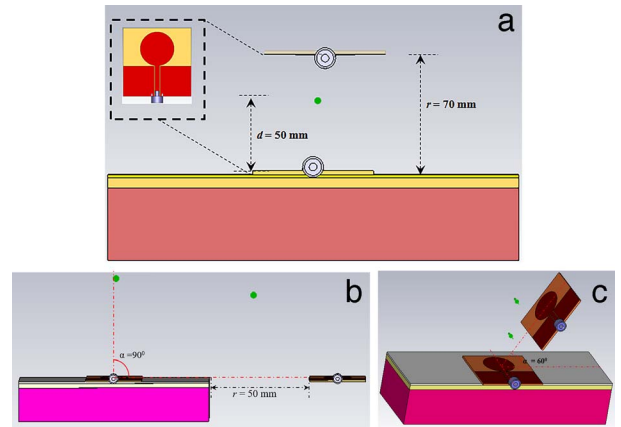


Figure 3. Arrangement of the on-body UWB monopole Tx mounted on a three-layered human phantom arm and an off-body Rx placed at far field at a distance of  $r = 70$  mm. An electric probe is placed at  $d = 50$  mm in the far field of the Tx. (a) Top aligned at  $\theta = 0^\circ$ , (b)  $\theta = 60^\circ$ , and (c)  $\theta = 90^\circ$ .

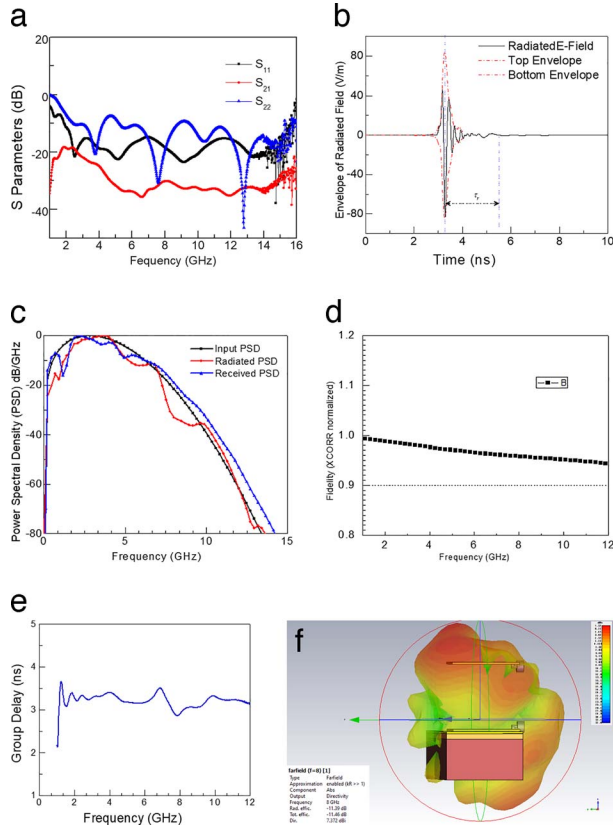


Figure 4. Frequency and time domain parameters for the arrangement shown in Figure 3a. (a) Frequency variation of  $S$  parameters over the impedance bandwidth 2 GHz to 12 GHz. (b) Radiated electric field sensed by the far-field electric probe placed in the Tx–Rx channel, as shown by the green dot in Figure 3a. Ringing interval  $\tau_r \sim 2.5$  ns. (c) PSD of input, radiated, and received pulses. (d) Computed fidelity between the input and received pulses. (e) Computation of group delay from the  $S_{21}$  characteristics. (f) The 3-D radiation pattern for 8 GHz.

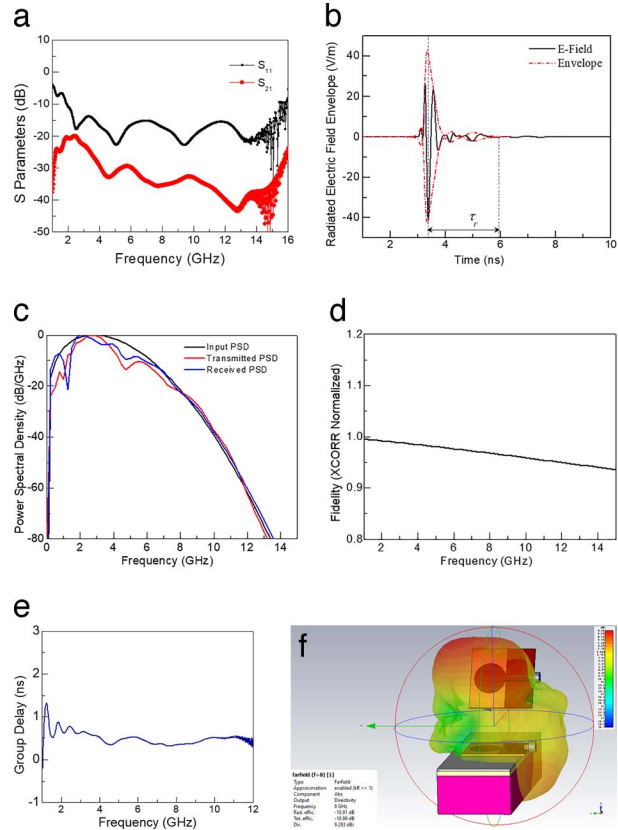


Figure 5. Frequency and time domain parameters for the arrangement shown in Figure 3b. (a) Frequency variation of  $S$  parameters over the impedance bandwidth 2 GHz to 12 GHz. (b) Radiated electric field sensed by the far-field electric probe placed in the Tx–Rx channel, as shown by the green dot in Figure 3b. Ringing interval  $\tau_r \sim 2.8$  ns. (c) PSD of input, radiated, and received pulses. (d) Computed fidelity between the input and received pulses. (e) Computation of group delay from the  $S_{21}$  characteristics. (f) The 3-D radiation pattern for 8 GHz.

computed by generating the envelope of the radiated field through the Hilbert transform, thereby calculating the time required for the peak of the envelope to fall to 5% of its peak value [17]. The  $\tau_r$  increases owing to the effect of the channel between Tx–Rx and the underlying phantom of the Tx. The three-dimensional (3-D) radiation plots shown in Figures 4f, 5f, and 6f are shown at 8 GHz, computed for three different cases of elevation.

Because of the antenna–body interactions, the radiation patterns become distorted unlike the pure omnidirectional one obtained for the stand-alone monopole in Figures 2e and 2f. Table 1 shows a comparative study of the pulse dispersion parameters, including the ringing interval, ringing ratio, maximum group delay, and radiation parameters, such as directivity and radiation efficiency. The ringing interval  $\tau_r$  and ringing ratio  $\tau_r/\tau$  changes when the height of the subcutaneous layer or the hypodermis made of fat grows thicker. It has been observed that  $\tau_r$  decreases with increase in  $h_2$ . This can be attributed to the reflections from an underlying thicker layer of a constant  $\epsilon_r$  being less compared to multiple

thinly layered substrates with a different  $\epsilon_r$ . Looking at how directivity increases with frequency due to reflections from the body for the different fat thickness, as in Table 1, it is observed that gain decreases considerably with frequency for respective fat thickness. This leads to decreased radiation efficiency, which is indeed expected for the on-body antenna, to prevent excessive radiation from tampering with the physiological body balance leading to hazardous biosafety issues.

Table 1. Comparison of pulse dispersion parameters and antenna radiation parameters with variation in fat thickness of the phantom model<sup>a</sup>

$h_2$ (mm)	$GD_M$ (ns)	$\tau_r$	$(\tau_r/\tau)$	Directivity		Radiation efficiency	
				5 GHz	8 GHz	5 GHz	8 GHz
5	3.60	1.78	4.45	6.28	6.99	-11.59	-13.18
10	3.52	1.59	3.975	4.9	7.58	-12.21	-13.14
15	3.5	1.47	3.675	5.78	7.39	-11.92	-13.33
20	3.4	1.34	3.35	6.27	7.48	-10.81	-12.84

<sup>a</sup>  $GD_M$ : maximum group delay;  $\tau_r$ : ringing interval,  $\tau$ : pulse width;  $\tau_r/\tau$ : ringing ratio.

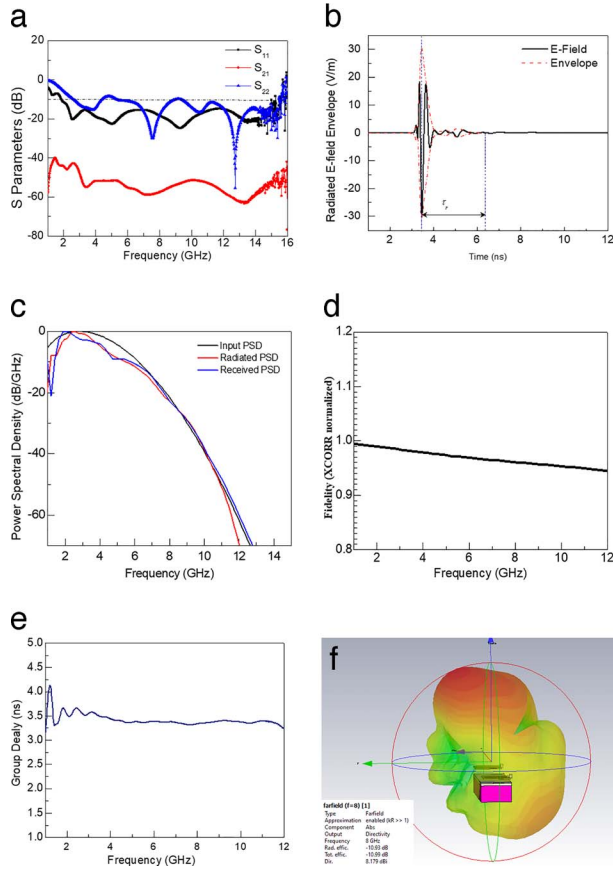


Figure 6. Frequency and time domain parameters for the arrangement shown in Figure 3c. (a) Frequency variation of  $S$  parameters over the impedance bandwidth of 2 GHz to 12 GHz (b) Radiated electric field sensed by the far-field electric probe placed in the Tx-Rx channel, as shown by the green dot in Figure 3c. Ringing interval  $\tau_r \sim 2.2$  ns. (c) PSD of input, radiated, and received pulses. (d) Computed fidelity between the input and received pulses. (e) Computation of group delay from the  $S_{21}$  characteristics. (f) The 3-D radiation pattern for 8 GHz.

### 3.2 Experimental Findings

The experimental setup used for measurement is shown in Figure 7a, where the Tx antenna has been attached on a female volunteer with a height of 157 cm and weight of 54 kg. Measured  $S_{21}$  magnitude variations with frequency for various elevation angles in the far field are shown in Figure 7b, and the computed group delay curve is shown in Figure 7c. The magnitude scale of both measured  $S_{21}$  and group delay differ from the simulation, which can be attributed to the spurious reflections in measurement setup that might have occurred when the off-body antenna was given external support to maintain stability.

### 4. Conclusion

In this article, a pulse dispersion estimation approach for UWB channel modeling is presented, which utilizes thorough analysis of transient figures of merit in terms of ringing interval, ringing ratio, and

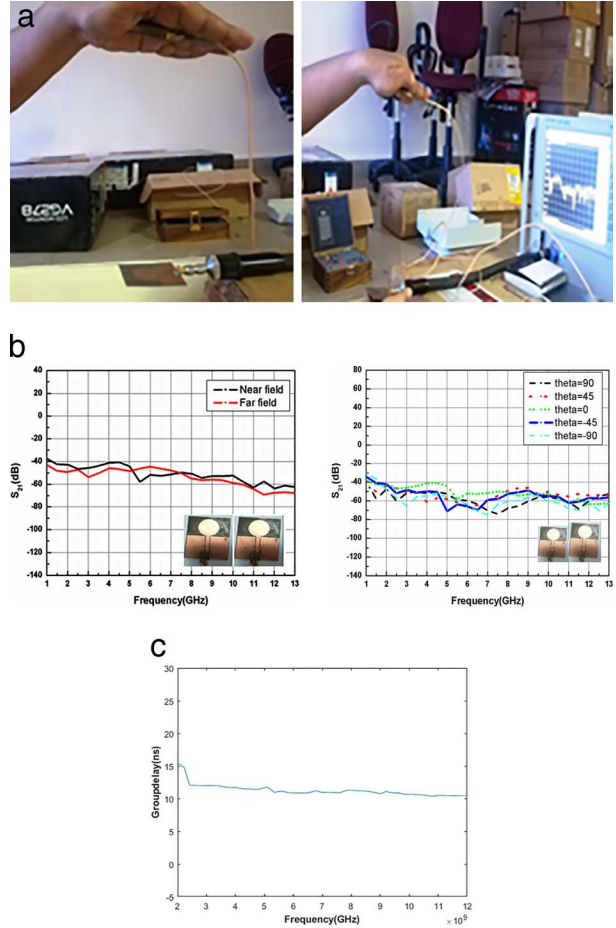


Figure 7. (a) Experimental setup with an on-body antenna and an off-body antenna kept in the palm of the volunteer. (b)  $S_{21}$  characteristics for various scenarios: near-field, far-field, and elevation angle variation. (c) Computation of group delay from experimentally available complex  $S_{21}$  data.

group delay. The presented scheme of obtaining the fidelity between the input and received short pulses seems to be the easiest and a promising alternative to the stochastic channel estimation approach. Deep insight into the effect of the three-layered phantom tissue environment on pulse dispersion and antenna radiation characteristics is presented in Table 1 for the different thickness of the hypodermal fat layer. The CIRs for various channel scenarios, such as LOS, NLOS, dynamic, static, indoor and outdoor, are currently being obtained experimentally and will be reported shortly for further validation of the proposed methodology.

### 5. References

1. N. Chahat, M. Zhadobov, R. Sauleau, and K. Ito, "A Compact UWB Antenna for On-Body Applications," *IEEE Transactions on Antennas and Propagation*, **59**, 4, April 2011, pp. 1123-1131.
2. C. Briso, C. Calvo, and Y. Xu, "UWB Propagation Measurements and Modelling in Large Indoor Environ-

- ments,” *IEEE Access*, **7**, March 2019, pp. 41913-41920, doi: 10.1109/ACCESS.2019.2905142.
3. S. Cotton, R. D’Ericco, and C. Oestges, “A Review of Radio Channel Models for Body Centric Communications,” *Radio Science*, **49**, 6, June 2014, pp. 371-378.
  4. Z. Irahauten, H. Nikookar, and G. J. M. Janssen, “An Overview of Ultra Wide Band Indoor Channel Measurements and Modeling,” *IEEE Microwave and Wireless Components Letters*, **14**, 8, August 2004, pp. 386-388.
  5. A. Alomainy, Y. Hao, X. Hu, C. G. Parini, and P. S. Hal, “UWB On-Body Radio Propagation and System Modeling for Wireless Body-Centric Networks,” *IEEE Proceedings-Communications*, **153**, 1, February 2006, pp. 107-114.
  6. Q. Wang, T. Tayamachi, I. Kimura, and J. Wang, “An On-Body Channel Model for UWB Body Area Communications for Various Postures” *IEEE Transactions on Antennas and Propagation*, **57**, 4, April 2009, pp. 991-998.
  7. T. S. P. See and Z. Chen, “Experimental Characterization of UWB Antennas for On-Body Communications,” *IEEE Transactions on Antennas and Propagation*, **57**, 4, April 2009, pp. 866-874.
  8. A. Alomainy, A. Sani, A. Rahman, J. G. Santas, and Y. Hao, “Transient Characteristics of Wearable Antennas and Radio Propagation Channels for Ultrawideband Body-Centric Wireless Communications,” *IEEE Transactions on Antennas and Propagation*, **57**, 4, April 2009, pp. 875-884.
  9. A. Sani, A. Alomainy, G. Palikaras, Y. Nechayev, Y. Hao, et al., “Experimental Characterization of UWB On-Body Radio Channel in Indoor Environment Considering Different Antennas,” *IEEE Transactions on Antennas and Propagation*, **58**, 1, January 2010, pp. 238-241.
  10. K. Ito, N. Haga, M. Takahashi, and K. Saito, “Evaluations of Body-Centric Wireless Communication Channels in a Range From 3MHz to 3 GHz,” *Proceedings of the IEEE*, **100**, 7, July 2012, pp. 2356-2363.
  11. A. Maskooki, C. Boon, E. Gunawan, and K. S. Low, “Ultra-Wideband Real-Time Dynamic Channel Characterization and System-Level Modeling for Radio Links in Body Area Networks,” *IEEE Transactions on Microwave Theory and Techniques*, **61**, 8, August 2013, pp. 2995-3004.
  12. Q. Zhang, J. Sarrazin, M. Casaletti, P. De Doncker, and A. Benlarbi-Dela, “Assessment of On-Body Skin-Confined Propagation for Body Area Network,” *IEEE Antennas and Wireless Propagation Letters*, **16**, August 2017, pp. 2610-2613, doi: 10.1109/LAWP.2017.2735631.
  13. R. Bharadwaj and S. K. Koul, “Experimental Analysis of Ultra-Wideband Body-to-Body Communication Channel Characterization in an Indoor Environment,” *IEEE Transactions on Antennas and Propagation*, **67**, 3, March 2019, pp. 1779-1789.
  14. R. Dautov and G. R. Tsouri, “Dynamic Off-Body Rician Channel Modeling for Indoor Wireless Body Area Networks,” *IEEE Journal of Biomedical and Health Informatics*, **24**, 5, May 2020, pp. 1246-1254.
  15. Computer Simulation Technology, *CST Microwave Studio*, version 2018, City, State or Country, Publisher, <http://Xxxx.Xxxxx>, 2018.
  16. MathWorks, *MATLAB*, version X, Natick, MA, USA, MathWorks, <http://Xxxx.Xxxxx>, 2010.
  17. D. Mandal and S. S Pattnaik, “Quad Band Wearable Slot Antenna With Low SAR Values for 1.8 GHz DCS, 2.4 GHz WLAN and 3.6/5.5 GHz WiMax Applications,” *Progress in Electromagnetic Research B*, **81**, January 2018, pp. 163-182, doi: 10.2528/PIERB18052504.
  18. D. Ganguly, D. Guha, S. Das, and A. Rojatkhar, “Systematic Approach to Estimating Monocycle Pulse for Time Domain Studies of UWB Antennas Using Numerical Computations and Simulation Tools,” *IEEE Antennas Propag. Magazine*, **56**, 4, August 2014, pp. 73-87.